ACS Catalysis

pubs.acs.org/acscatalysis Letter

Sequence Rules the Functional Connections and Efficiency of Catalytic Precision Oligomers

Jie Li, Qian Qin, Sinan Kardas, Mathieu Fosségré, Mathieu Surin,* Antony E. Fernandes, Karine Glinel, and Alain M. Jonas*

Cite This: *ACS Catal.* 2022, 12, 2126–2131 Read Online

ACCESS | Metrics & More | Article Recommendations | Supporting Information

ABSTRACT: The efficiency of cooperative catalysts is dependent on the probabilities of chance encounter between the different complementary catalytic units. Connecting these catalytic groups along a short flexible oligomeric chain increases these probabilities. Here, we show that the sequence of a catalytic triad precisely positioned along a flexible backbone also strongly matters, with the catalytic activity varying by up to 1 order of magnitude when interchanging two groups in the oligomer sequence. These results are rationalized with molecular graphs computed from molecular dynamics simulations, showing how functional connections between catalytic groups are dependent on sequence order.

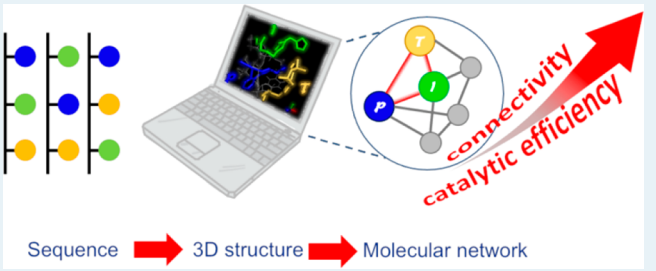

KEYWORDS: *Multifunctional catalysis, precision oligomers, aerobic oxidation, alcohols, graph theory*

In multifunctional catalysis,[1] an ideal positioning of the cooperatively involved catalytic groups is key for an optimized efficiency. A seminal example is provided by enzymatic catalysis, which relies on the precise positioning of catalytic groups on the three-dimensional framework of the tertiary structure of the protein. Similarly, in supported catalysis, surface attachment provides the constraining framework, allowing one to optimize the relative locations and interactions of the catalytic groups, leading to significant improvements of catalytic activity.[2−7] As a particular example, connecting the groups in a precise sequence along oligomeric chains densely grafted on a surface results in the fine-tuning of interchain cooperative interactions and an optimized catalytic activity.[8]

In homogeneous multifunctional catalysis, however, the efficiency is dependent on the probabilities of chance encounters between the different moieties, that vary with concentration, temperature, and specific interactions between the soluble catalytic groups. By connecting the different catalytic groups at specific locations along a short oligomeric chain, the local probabilities of encounter may strongly increase, compared to the free monomeric system in solution. Previous work in this field is scarce and concentrated on peptoid[9] or peptidomimetic[10] chains bearing two catalytic functional groups at various locations in the sequence. Whereas the remarkable efficiency of some of these systems often results from the formation of secondary structures which bring the functional groups in close spatial proximity, it may also result from the biasing of the probability of chance encounters between the groups due to the constraints set by the backbone and the presence of inactive units along the chain, in the absence of secondary structures.[9] In this case, this requires the conformational freedom of the chain to be large enough for the involved groups to be able to meet in space.

Conformational freedom is also needed to increase the configurational entropy of the solution, which is required for solubility in homogeneous catalysis. However, one might think that conformational diversity associated with thermal fluctuations will strongly blur the effect of the sequence of the chain-grafted catalytic groups, especially when the number of involved catalytic units increases. In contrast, here, we show that the catalytic efficiency of flexible trifunctional catalytic precision oligomers can vary by a factor of up to 10 when simply interchanging two active sites in the sequence. We explain these remarkable results with network analysis applied to the average chain conformation extracted from molecular dynamics (MD) simulations that show that, although the average spatial distance/proximity between the groups of the catalytic triad remains identical, irrespective of sequence, the catalytic cooperation is affected by the interposition of noncatalytic segments of the oligomers, which limits the probability of formation and accessibility of the active triad, all of which is ruled by sequence. Thereby, we demonstrate, for

Received: December 3, 2021
Revised: January 23, 2022
Published: January 26, 2022

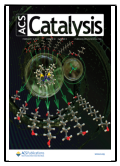

https://doi.org/10.1021/acscatal.1c05560
ACS Catal. 2022, 12, 2126−2131

the first time, the interest of graph theory for the prediction of the catalytic activity of sequence-defined oligomers.[11,12]

The reference multifunctional catalytic system selected for our conceptual demonstration consists of 2,2,6,6-tetramethyl-1-piperidinyloxyl (TEMPO), imidazole, and a pyridyltriazol (pyta)-Cu complex for the selective aerobic oxidation from alcohols to aldehydes.[13−16] The propensity of the imidazole site to reach the copper site is critical for enabling high turnovers,[5,6] this being most probably linked to the formation of a pyta-Cu-imidazole complex with decreased redox potential favoring O_2 activation, TEMPO being subsequently involved in the electron cascade.[15] Previously,[8] we investigated the effect of sequence on the catalytic activity of grafted chains of two discrete oligomers bearing this catalytic triad. We showed the importance of sequence and surface confinement in orchestrating the interactions of the triad, whose catalytic activity was dominated by surface-enhanced interchain interactions rather than purely sequence-encoded intrachain cooperativity. In this preliminary study, we also analyzed the catalytic properties of the free chains. Yet, the synthetic scheme did not allow us to prepare all interesting sequences and, thus, to fully probe the effect of primary structure of multifunctional catalytic oligomers. In addition, the relative importance of interchain and intrachain interactions could not be estimated. Finally, the chain backbone was of limited flexibility, which reduced the probability of chance encounters. As a result, the effect of sequence on catalytic activity remains an open issue for nongrafted flexible chains.

Here, we therefore adopt a different synthetic scheme[17] leading to an easier integration and positioning of functional units along a more flexible backbone. Especially, we take advantage of the powerful "click" copper-catalyzed azide−alkyne cycloaddition (CuAAC) reaction for both the functional group insertion and chain elongation steps, providing a robust access to all possible sequences of the oligomeric catalytic triad (see Scheme S1 in the Supporting Information). Out of the six possible sequences (given the directionality of the backbone that starts by a protected alkyne and ends by a benzyl carbamate), we selected three "nonsymmetric" representative sequences, namely, **TIP**, **TPI**, and **ITP** (Scheme 1) to examine our concept. The oligomers **TIP**, **TPI**, and **ITP** were synthesized following a previously published route (Scheme S1), with reasonable average yields (16%, 20%, and 23% for **TIP**, **TPI**, and **ITP**, respectively, starting from the monomer units). Additionally, we also synthesized the **T**, **I**, **P** monomer units, and **PI** and **TP** dimer units as references (SI for synthesis and characterization data).

We first checked that the single monomers do not catalyze the aerobic oxidation of benzyl alcohol (BnOH) into benzaldehyde at 60 °C, using a copper loading of 2.5 mol %, relative to benzyl alcohol and a 1:1 CuI:monomer molar ratio (see the Supporting Information for details on the catalytic experiments). Benzaldehyde yields were negligible for the three monomers after 60 min reaction time, with values of 0, 0.15%, and 0.01% for monomers **T**, **I**, and **P**, respectively (Figure S67 in the Supporting Information). Two dimers containing the copper-binding **P** ligand but lacking one of the two other units were also tested, with again very low yields of benzaldehyde (0.92% and 0.51% after 60 min for dimers **PI** and **TP**, respectively; see Figure S67). Upon addition of a stoichiometric amount of **T** to **PI**, or of **I** to **TP**, the yields increased significantly by a factor of ca. 5 to 4.1% and 2.9% after 60 min, respectively (see Figure S68 in the Supporting Information).

Scheme 1. Catalytic Trimers, Dimers, and Monomers

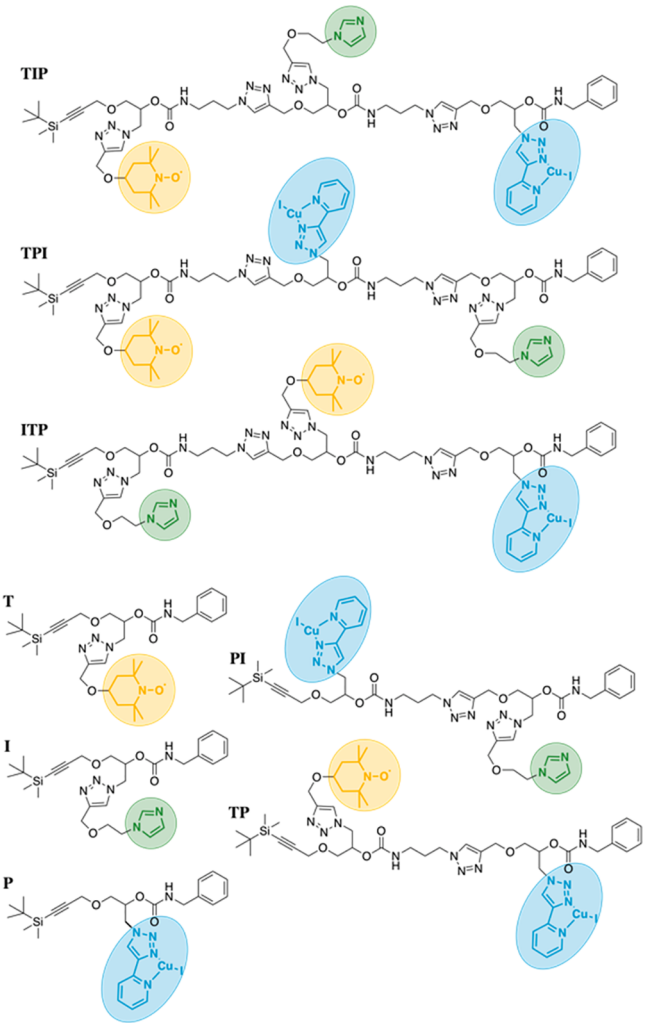

These preliminary experiments confirm that cooperativity between the three units is required for efficiency.

NMR spectra of the **PI** dimer were taken in the presence of 0.5 and 1 equiv of CuI, to visualize how copper interacts with the numerous nitrogen-rich groups of the oligomers (see Figures S24 and S25 in the Supporting Information). All protons associated with the pyta group (blue circle in Scheme 1) disappeared in the presence of copper, indicating that these protons are in the intermediate exchange rate regime at the NMR time scale, because of the formation of a strong complex with copper. The protons of the imidazole group (green circle in Scheme 1) also disappeared, confirming that NMI acts as a complementary ligand in this catalytic complex. In contrast, the protons of the triazole and carbamate groups of the backbone were simply shifted, showing that these protons are in the fast exchange rate regime; therefore, triazole and carbamate groups interact with copper but do not form a long-lived complex with copper. Hence, the triazole and carbamate linkers are essentially spectators to catalysis (except for the triazole of the pyta group).

The sequence-defined catalytic oligomers **TIP**, **TPI**, and **ITP** were then tested in the same reaction (Figure 1; see the Supporting Information for details). Different copper loadings were investigated (1, 2.5, and 5 mol %, relative to benzyl alcohol), always keeping a 1:1 CuI:oligomer molar ratio, in

https://doi.org/10.1021/acscatal.1c05560
ACS Catal. 2022, 12, 2126−2131

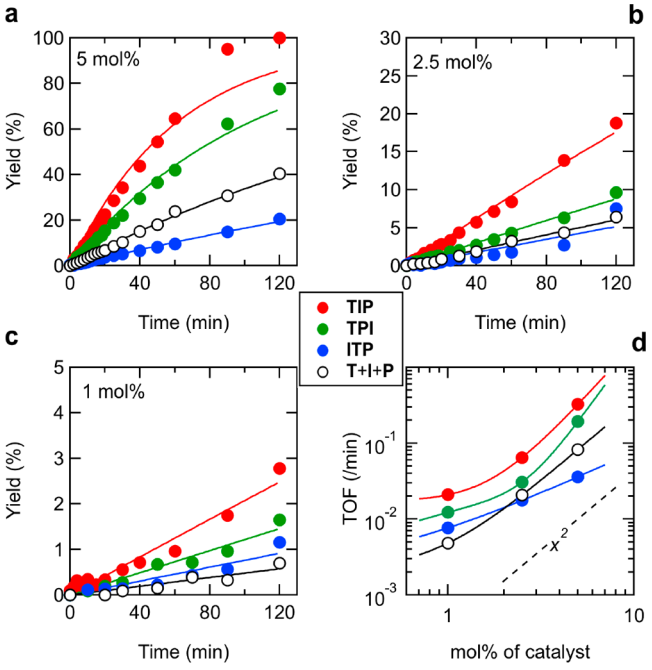

Figure 1. (a–c) Catalytic activity of **TIP**, **TPI**, **ITP** oligomers and the equimolar mixture of **T**, **I**, and **P** monomers in the aerobic oxidation of BnOH into benzaldehyde; reactions were performed using different loadings of the catalytic oligomers and CuI (with a 1:1 oligomer:Cu molar ratio); yields correspond to the measured molar concentration of benzaldehyde, relative to the initial molar concentration of BnOH. The curves are fits to a first-order kinetic equation over the complete sets of data. (d) Corresponding turnover frequencies (TOFs) depending on loading, computed from the apparent rate constant extracted from the fits. Curves are drawn to guide the eye. The dashed line is a square power law. Full conditions and numerical data are provided in the Supporting Information.

order to vary the relative balance of interchain and intrachain interactions. From MD simulations, all trimers have an average radius of gyration of R_G = 0.66 nm (Figure S57 in the Supporting Information). Consequently, all catalytic chains are in the dilute regime with the average distance between coils ranging from ca. $8R_G$ to $14R_G$ for 5 and 1 mol % copper loading, respectively. At 1 mol %, the average volume of solution available per chain is, thus, ca. 650 (= $14^3/(4\pi/3)$) times larger than the average volume of the chain; hence, interchain interactions start to be negligible at this concentration.

Impressively, a strong effect of sequence was detected, with 5 mol % **TIP** providing complete conversion in 120 min, while **TPI** and **ITP** led to only 78 and 21% yield after the same period (Figure 1a). Despite chain flexibility, selecting the proper sequence may thus significantly improve (**TIP**, **TPI**) or deteriorate (**ITP**) catalytic activity compared to the mixture of individual monomers **T** + **I** + **P** (Scheme 1) that provided only 40% conversion after 120 min under identical conditions (Figure 1a). Decreasing the loading from 5 to 2.5 and 1 mol % resulted in a significant slowing down of the reaction, yet with a preservation of the relative order of efficiency for the three discrete catalysts (Figures 1b and 1c), namely **TIP** > **TPI** > **ITP**. For the lowest loading (1 mol %), all oligomers outperformed the separated system. The same relative order of efficiency was found for the aerobic oxidation of *trans* 2-hexen-1-ol into *trans* 2-hexen-1-al, albeit from 2 to 4 times slower than for benzyl alcohol (Figure S69 in the Supporting Information). Of note, catalytic experiments performed with the TBDMS-deprotected oligomers were partly impaired by concomitant oxidative Glaser–Hay coupling[18−20] between the alkyne-terminated chains (see Figure S53 in the Supporting Information); therefore, only TBDMS-protected oligomers are considered in this work.

A first-order kinetic equation was fit to the data (yield $Y = 1 - \exp(-k_{obs}\, t)$ with k_{obs} being the apparent rate constant and t the reaction time; see Figures 1a–c); because the data started to deviate from this expression at high conversion, we also computed the rate constants from the initial slopes of the yield curves (for $Y < 0.35$ and $t \leq 90$ min; see Figures S64a–S64c in the Supporting Information). Conventional linearized plots of $\ln(1 - Y)$ vs t are also reported in the Supporting Information (Figures S65a–S65c), together with linear fits performed over the complete range or for low conversions (Figure S66a–c in the Supporting Information); the different values obtained for k_{obs} by these four different fitting procedures are reported in Table S2 in the Supporting Information, together with standard errors. The turnover frequencies (TOFs) were then computed by dividing k_{obs} by x_{mol}, the copper loading expressed in molar fraction of the initial alcohol concentration (see Figure 1d, as well as Figures S64d, S65d, and S66d and Table S2 in the Supporting Information).

For the separated system made of the three monomer units **T** + **I** + **P**, the TOF varies approximately as x_{mol}^2, indicating a third-order dependence of the reaction rate on loading (Figure 1d). Previous studies concluded that the rate-determining step for the oxidation of benzyl alcohol in acetonitrile in the presence of bipyridine, $Cu^{(I)}$, NMI, and TEMPO is the oxidation of the copper complex, with the formation of an intermediate Cu_2O_2 species involving two Cu atoms, resulting in a mixed second- and first-order dependence of the reaction rate on copper concentration, and in a first-order dependence on oxygen partial pressure.[13,16] In contrast, the subsequent oxidation steps involving TEMPO and the alcohol were found not to be rate-determining, resulting in a zero-order dependence on the concentration of TEMPO and alcohol. Given our conditions in which **T**, **P**, **I**, and $Cu^{(I)}$ are introduced in stoichiometric amounts, with constant oxygen pressure and fixed initial alcohol concentration, these predictions should lead to a TOF proportional to x_{mol} at low catalyst concentrations, and to a constant TOF at high concentrations in catalyst, which is not observed here. Furthermore, since our preliminary experiments at 2.5 mol % catalyst indicated an increase of kinetics by a factor of ca. 5 upon adding **T** to **PI** or **I** to **TP** (Figures S67 and S68 in the Supporting Information), the rate equation must be dependent on the concentrations of **T** and **I**, which also deviates from previous findings. Our results thus significantly differ from these previous studies, indicating that the catalytic mechanism may differ for the present system, compared to previous ones. Systematic studies in which the concentrations of copper, **T**, **I**, and **P** are varied independently would be needed to progress further in this issue.

Although normalized per catalyst content, the TOFs of the trimer-based systems also increase with catalyst concentration, showing that chance encounters between chains still play a beneficial role in our conditions. However, the concentration dependence levels off at higher dilutions, when trimers become more efficient than the system made of the three separated monomer units. Crucially, in this very dilute regime, the catalytic efficiency of the trimers is still strongly dependent on the sequence order of the chains. This hints to the existence of

https://doi.org/10.1021/acscatal.1c05560
ACS Catal. 2022, 12, 2126−2131

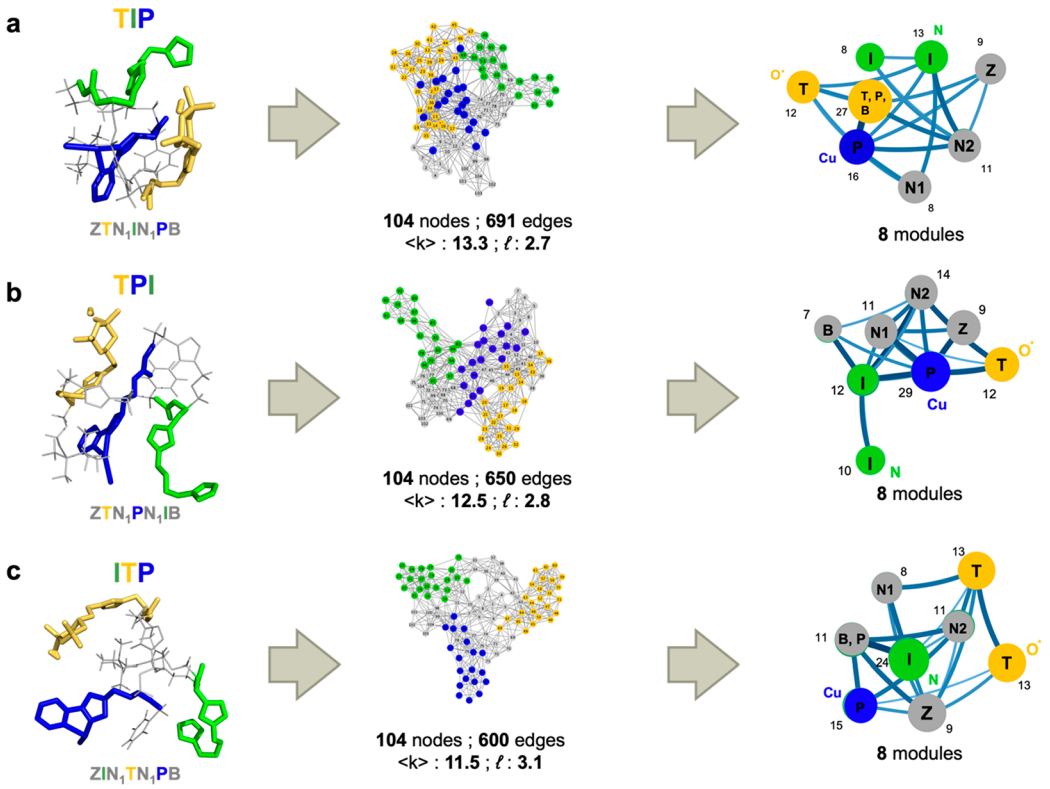

Figure 2. Left: Final MD snapshots of (a) **TIP**; (b) **TPI**; and (c) **ITP** sequences (in sticks representation). The **T**, **P**, and **I** units are depicted in yellow, blue, and green, respectively. Z, N_1, N_2, and B are the noncatalytic groups represented in gray in the Supporting Information. Middle: Network representation of the corresponding sequences, with the topological descriptors of the networks. Colors correspond to the catalytic units represented on the left. **Right:** Modularization of the oligomer networks for the corresponding sequences. The circles represent the modules of highly connected nodes. The letters of each fragment associated with the modules are shown, as well as the representative atoms of the catalytic units. The size of the circles is proportional to the number of nodes, annotated next to the modules. The thickness of the edges (lines) is proportional to the degree of connectivity between the modules.

a chain-intrinsic catalytic regime, in which interchain interactions are limited and catalysis essentially occurs by the cooperative interactions between the three units of the chains. The TOF values obtained by the four different kinetic fits, although slightly different in absolute value, provide similar conclusions with respect to the relative ordering of the efficiency of the catalysts. Comparable results were also obtained for the oxidation of *trans* 2-hexen-1-ol (Figure S69 in the Supporting Information).

These results indicate that sequence plays an important role, even at very low dilution when interchain interactions strongly decrease, despite the presence of linear aliphatic segments along the backbone, which provides significant flexibility to the chains. This large flexibility was confirmed by all-atom MD simulations performed in implicit acetonitrile solvent over 1 μs time scale (with a 1 fs time step), which indicated structures folded into compact globular shapes. The root-mean-square fluctuation (RMSF) profiles showed a similar conformational dynamics for the three oligomers with a high overall flexibility (average RMSF of ca. 0.7 nm),[21,22] regardless of the sequence (Figure S55 in the Supporting Information). The flexibility of the oligomeric chains is also evident from the large variations of the chain end-to-end distances with simulation time, from 0.4 nm to ca. 2.3 nm (Figure S56 in the Supporting Information). Nevertheless, the chain-ends that are far apart in the primary sequence remain, on average, close in the 3D structure (average chain end-to-end distances of ca. 0.9 nm), regardless of the sequence (Figure S56). On average, these chain ends are located at the periphery of the globular structure, given that the average diameter of gyration is ∼1.3 nm for all trimers; hence, chain ends are unlikely to interpose between the catalytic groups of the chains.

A large conformational sampling through MD simulations showed that both the average distances between the catalytic units and the distributions of the area of the triangle formed by the three catalytic units are not strongly influenced by the sequence order (Table S1 and Figure S58 in the Supporting Information). Hence, these simple geometrical descriptors could not explain the different catalytic activity for the three sequences. To further understand why and how sequence order plays such a role in our flexible trifunctional chains, graph theory was used to analyze results from MD simulations.[23−25] Molecular graphs were drawn from the average conformations of the oligomers obtained from the MD simulations to decipher the role of the intrachain organization (see Figure 2).

Clearly, the connectivity between the nodes of the catalytic units (colored circles in Figure 2, middle) are strikingly different for the three oligomers, the most connected to the least connected catalytic triads being **TIP** > **TPI** > **ITP**. The average degree ($\langle k \rangle$) and the characteristic path length (l)) of the molecular networks were used as topological descriptors (Section 9 in the Supporting Information). The networks have an average degree $\langle k \rangle$ of 13.3, 12.5, and 11.5 and a characteristic path length l of 2.7, 2.8, and 3.1 for **TIP**, **TPI**, and **ITP** sequences, respectively. Both the decrease of $\langle k \rangle$ and

https://doi.org/10.1021/acscatal.1c05560
ACS Catal. 2022, 12, 2126−2131

the increase of *l* indicate that some regions of the oligomers are less connected and more isolated from each other depending on the sequence. Modularization of the molecular graphs (Figure 2 right and Supporting Information) allows us to detect the connections between the three catalytic units and thus their ability to act cooperatively. While the number of modules (*i.e.*, intraconnected regions) was the same for the three sequences, the number of nodes in each modules were influenced by the sequence. For both the **TIP** and **TPI** sequences (Figure 2a and 2b), the catalytic modules **T**, **I**, and **P** (i.e., modules made of nodes corresponding to the catalytic fragments) remain highly connected, without noncatalytic modules (in gray in Figure 2, right) that interfere between them. The oligomers are thus intrinsically folded in such a way that the three catalytic units **T**, **I**, and **P** are in proximity and connected. In contrast, for the **ITP** sequence (Figure 2c), the **T** nodes are connected to **I** and **P** modules via a few intermediate nodes, meaning that they are screened by the noncatalytic fragments in the chain organization. Globally, the network topologies shown in Figure 2 correlate well with the measured catalytic activities of the oligomers: the **TIP** sequence is the most catalytically active and the **ITP** sequence is the least catalytically active, while the **TPI** sequence represents an intermediate case. This demonstrates that the sequence is of tremendous importance to organize in an efficient way the three catalytic units. Obviously, interchain interactions will add a supplementary degree of complexity when concentration increases, which would warrant complementary studies.

Finally, to probe the driving force for oligomer folding, we estimated the number of hydrogen bonds between the carbamate groups in the oligomer backbones, and between the triazole groups, which are good mimetics of secondary amides regarding hydrogen-bonding abilities.[26] For the three oligomers, the number of hydrogen bonds in each conformation evolves from 0 to 2 (in rare cases, 3), and no hydrogen bond is persistent for more than 10% of the simulation time (Figure S59 in the Supporting Information). Therefore, hydrogen bonding contributes only weakly to the globular folding of the oligomers. In contrast, the numerous aromatic rings along the oligomer backbone and on the side chains provide many possibilities of aromatic interactions. Those include 23 persistent aromatic interactions present over 50% of the simulation time, with a more important contribution of interactions between lateral groups (Figures S60−S62 in the Supporting Information). Therefore, the aromatic interactions are the dominant forces of the globular folding and intrachain organization, as observed for related oligomers.[17] Altogether, these results suggest that the understanding of the spatial arrangement and connections between the catalytic units through conformational sampling could leverage the optimization of catalytic activities in precision oligomers.

In conclusion, the probability to combine, in a multifunctional active site, three catalytic units ordered within an oligomeric chain is strongly dependent on sequence, even for chains of significant conformational flexibility. Despite blurring by random conformational fluctuations, intrachain-excluded volume interactions still bias the probability landscape, which may result in differences of TOFs as large as 1 order of magnitude at higher loadings. Therefore, and somewhat counterintuitively, the flexibility of the framework supporting the catalytic units is not necessarily an issue and may be used to boost catalytic efficiency. Conversely, an inadequate sequence of catalytic units may result in a poorer efficiency than the simple free mixture of individual catalytic components. Given the high flexibility of our backbones, it is unlikely that longer spacers would lead to significant differences in the catalytic efficiency. On the other hand, reducing their length or stiffening the backbone might be counterproductive, by decreasing the probability of encounter of the catalytic groups; this remains to be demonstrated experimentally or by making use of molecular graphs computed from MD simulations that pictorially describe the interactions and connections between the catalytic units as required for multifunctional catalysis. Therefore, the use of such molecular network representations is an important asset for the design of even improved multifunctional homogeneous catalysts.

■ ASSOCIATED CONTENT

Supporting Information

The Supporting Information is available free of charge at https://pubs.acs.org/doi/10.1021/acscatal.1c05560.

Synthetic procedures, characterization data, experimental methods, computational details, and network analysis (PDF)

■ AUTHOR INFORMATION

Corresponding Authors

Mathieu Surin − *Laboratory for Chemistry of Novel Materials, Centre of Innovation and Research in Materials and Polymers (CIRMAP), University of Mons - UMONS, 7000 Mons, Belgium;* orcid.org/0000-0001-8950-3437; Email: alain.jonas@uclouvain.be

Alain M. Jonas − *Institute of Condensed Matter and Nanosciences, Bio- and Soft Matter, Université Catholique de Louvain, 1348 Louvain-la-Neuve, Belgium;* orcid.org/0000-0002-4083-0688; Email: mathieu.surin@umons.ac.be

Authors

Jie Li − *Institute of Condensed Matter and Nanosciences, Bio- and Soft Matter, Université Catholique de Louvain, 1348 Louvain-la-Neuve, Belgium*

Qian Qin − *Institute of Condensed Matter and Nanosciences, Bio- and Soft Matter, Université Catholique de Louvain, 1348 Louvain-la-Neuve, Belgium*

Sinan Kardas − *Laboratory for Chemistry of Novel Materials, Centre of Innovation and Research in Materials and Polymers (CIRMAP), University of Mons - UMONS, 7000 Mons, Belgium; Institute for Complex Molecular Systems, Eindhoven University of Technology - TU/e, Eindhoven 5600 MB, The Netherlands;* orcid.org/0000-0002-4532-8160

Mathieu Fosséprè − *Laboratory for Chemistry of Novel Materials, Centre of Innovation and Research in Materials and Polymers (CIRMAP), University of Mons - UMONS, 7000 Mons, Belgium*

Antony E. Fernandes − *Certech, 7180 Seneffe, Belgium;* orcid.org/0000-0002-7993-2980

Karine Glinel − *Institute of Condensed Matter and Nanosciences, Bio- and Soft Matter, Université Catholique de Louvain, 1348 Louvain-la-Neuve, Belgium;* orcid.org/0000-0002-2000-0169

Complete contact information is available at:

https://doi.org/10.1021/acscatal.1c05560
ACS Catal. 2022, 12, 2126−2131

https://pubs.acs.org/10.1021/acscatal.1c05560

Notes

The authors declare no competing financial interest.

■ ACKNOWLEDGMENTS

The authors acknowledge the Fonds de la Recherche Scientifique - FNRS and the Fonds Wetenschappelijk Onderzoek, under EOS Project No. 30650939 for financial support. Computational resources have been provided by the Consortium des Équipements de Calcul Intensif (CÉCI), funded by FNRS (Grant No. 2.5020.11) and Wallonia Region. The authors acknowledge Gabriella Barrozino-Consiglio for 500 MHz NMR analysis, Raoul Rozenberg for APCI-MS, Hervé Degand for ESI-MS/MS analysis, and Laurent Collard for GC analysis. K.G. and M.S. are Senior Research Associates of the F.R.S.−FNRS.

■ REFERENCES

(1) Martínez, S.; Veth, L.; Lainer, B.; Dydio, P. Challenges and Opportunities in Multicatalysis. *ACS Catal.* **2021**, *11* (7), 3891−3915.
(2) Motokura, K. Multifunctional Solid Surfaces for Enhanced Catalysis. *ChemCatChem.* **2014**, *6* (11), 3067−3068.
(3) Margelefsky, E. L.; Zeidan, R. K.; Davis, M. E. Cooperative Catalysis by Silica -Supported Organic Functional Groups. *Chem. Soc. Rev.* **2008**, *37* (6), 1118−1126.
(4) Díaz, U.; Brunel, D.; Corma, A. Catalysis Using Multifunctional Organosiliceous Hybrid Materials. *Chem. Soc. Rev.* **2013**, *42* (9), 4083−4097.
(5) Chandra, P.; Jonas, A. M.; Fernandes, A. E. Spatial Coordination of Cooperativity in Silica-Supported Cu/TEMPO/Imidazole Catalytic Triad. *ACS Catal.* **2018**, *8* (7), 6006−6011.
(6) Fernandes, A. E.; Jonas, A. M. Design and Engineering of Multifunctional Silica-Supported Cooperative Catalysts. *Catal. Today* **2019**, *334*, 173−186.
(7) Fernandes, A. E.; Riant, O.; Jensen, K. F.; Jonas, A. M. Molecular Engineering of Trifunctional Supported Catalysts for the Aerobic Oxidation of Alcohols. *Angew. Chem., Int. Ed.* **2016**, *128* (37), 11210−11214.
(8) Chandra, P.; Jonas, A. M.; Fernandes, A. E. Sequence and Surface Confinement Direct Cooperativity in Catalytic Precision Oligomers. *J. Am. Chem. Soc.* **2018**, *140* (15), 5179−5184.
(9) Prathap, K. J.; Maayan, G. Metallopeptoids as Efficient Biomimetic Catalysts. *Chem. Commun.* **2015**, *51*, 11096−11099.
(10) Girvin, Z. C.; Gellman, S. H. Exploration of Diverse Reactive Diad Geometries for Bifunctional Catalysis via Foldamer Backbone Variation. *J. Am. Chem. Soc.* **2018**, *140* (39), 12476−12483.
(11) Meier, M. A. R.; Barner-Kowollik, C. A New Class of Materials: Sequence-Defined Macromolecules and Their Emerging Applications. *Adv. Mater.* **2019**, *31* (26), 1806027.
(12) Aksakal, R.; Mertens, C.; Soete, M.; Badi, N.; Du Prez, F. Applications of Discrete Synthetic Macromolecules in Life and Materials Science: Recent and Future Trends. *Adv. Sci.* **2021**, *8*, 2004038.
(13) Hoover, J. M.; Ryland, B. L.; Stahl, S. S. Copper/TEMPO-Catalyzed Aerobic Alcohol Oxidation: Mechanistic Assessment of Different Catalyst Systems. *ACS Catal.* **2013**, *3* (11), 2599−2605.
(14) Hoover, J. M.; Stahl, S. S. Highly Practical Copper(I)/TEMPO Catalyst System for Chemoselective Aerobic Oxidation of Primary Alcohols. *J. Am. Chem. Soc.* **2011**, *133*, 16901−16910.
(15) Ryland, B. L.; McCann, S. D.; Brunold, T. C.; Stahl, S. S. Mechanism of Alcohol Oxidation Mediated by Copper(II) and Nitroxyl Radicals. *J. Am. Chem. Soc.* **2014**, *136* (34), 12166−12173.
(16) Hoover, J. M.; Ryland, B. L.; Stahl, S. S. Mechanism of Copper(I)/TEMPO-Catalyzed Aerobic Alcohol Oxidation. *J. Am. Chem. Soc.* **2013**, *135* (6), 2357−2367.
(17) Li, J.; Leclercq, M.; Fossepré, M.; Surin, M.; Glinel, K.; Jonas, A. M.; Fernandes, A. E. Discrete Multifunctional Sequence-Defined Oligomers with Controlled Chirality. *Polym. Chem.* **2020**, *11* (24), 4040−4046.
(18) Leophairatana, P.; Samanta, S.; De Silva, C. C.; Koberstein, J. T. Preventing Alkyne-Alkyne (i.e., Glaser) Coupling Associated with the ATRP Synthesis of Alkyne-Functional Polymers/Macromonomers and for Alkynes under Click (i.e., CuAAC) Reaction Conditions. *J. Am. Chem. Soc.* **2017**, *139* (10), 3756−3766.
(19) Jover, J.; Spuhler, P.; Zhao, L.; McArdle, C.; Maseras, F. Toward a Mechanistic Understanding of Oxidative Homocoupling: The Glaser−Hay Reaction. *Catal. Sci. Technol.* **2014**, *4* (12), 4200−4209.
(20) Hay, A. S. Oxidative Coupling of Acetylenes. *J. Org. Chem.* **1960**, *25* (7), 1275−1276.
(21) da Penha Valente, R. P.; de Souza, R. C.; de Medeiros Muniz, G.; Ferreira, J. E. V.; de Miranda, R. M.; Lima e Lima, A. H.; da Silva Gonçalves Vianez Junior, J. L. Using Accelerated Molecular Dynamics Simulation to Elucidate the Effects of the T198F Mutation on the Molecular Flexibility of the West Nile Virus Envelope Protein. *Sci. Rep.* **2020**, *10* (1), 9625.
(22) Dong, Y.; Liao, M.; Meng, X.; Somero, G. N. Structural Flexibility and Protein Adaptation to Temperature: Molecular Dynamics Analysis of Malate Dehydrogenases of Marine Molluscs. *Proc. Natl. Acad. Sci. U. S. A.* **2018**, *115* (6), 1274.
(23) David, L.; Thakkar, A.; Mercado, R.; Engkvist, O. Molecular Representations in AI-Driven Drug Discovery: A Review and Practical Guide. *J. Cheminformatics* **2020**, *12* (1), 56.
(24) Brinda, K. V.; Vishveshwara, S. A Network Representation of Protein Structures: Implications for Protein Stability. *Biophys. J.* **2005**, *89* (6), 4159−4170.
(25) Benson, N. C.; Daggett, V. A Comparison of Multiscale Methods for the Analysis of Molecular Dynamics Simulations. *J. Phys. Chem. B* **2012**, *116* (29), 8722−8731.
(26) Valverde, I. E.; Mindt, T. L. 1,2,3-Triazoles as Amide-Bond Surrogates in Peptidomimetics. *Chimia Int. J. Chem.* **2013**, *67*, 262−266.

https://doi.org/10.1021/acscatal.1c05560
ACS Catal. 2022, 12, 2126−2131